



UNIVERSITY OF LEEDS

This is a repository copy of  *$\pi$ -Conjugated Indole Dyads with Strong Blue Emission Made Possible by Stille Cross-Coupling and Double Fischer Indole Cyclisation*.

White Rose Research Online URL for this paper:  
<http://eprints.whiterose.ac.uk/113721/>

Version: Accepted Version

---

**Article:**

Garrote Canas, AM, Martsinovich, N and Sergeeva, NN [orcid.org/0000-0003-0008-1560](https://orcid.org/0000-0003-0008-1560)  
(2017)  *$\pi$ -Conjugated Indole Dyads with Strong Blue Emission Made Possible by Stille Cross-Coupling and Double Fischer Indole Cyclisation*. *ChemistrySelect*, 2 (8). pp. 2433-2438. ISSN 2365-6549

<https://doi.org/10.1002/slct.201700217>

---

© 2017 Wiley-VCH Verlag GmbH & Co. KGaA, Weinheim. This is the peer reviewed version of the following article: 'Garrote Canas, AM, Martsinovich, N and Sergeeva, NN (2017)  *$\pi$ -Conjugated Indole Dyads with Strong Blue Emission Made Possible by Stille Cross-Coupling and Double Fischer Indole Cyclisation*. *ChemistrySelect*, 2 (8). pp. 2433-2438', which has been published in final form at <https://doi.org/10.1002/slct.201700217>. This article may be used for non-commercial purposes in accordance with Wiley Terms and Conditions for Self-Archiving. Uploaded in accordance with the publisher's self-archiving policy.

**Reuse**

Unless indicated otherwise, fulltext items are protected by copyright with all rights reserved. The copyright exception in section 29 of the Copyright, Designs and Patents Act 1988 allows the making of a single copy solely for the purpose of non-commercial research or private study within the limits of fair dealing. The publisher or other rights-holder may allow further reproduction and re-use of this version - refer to the White Rose Research Online record for this item. Where records identify the publisher as the copyright holder, users can verify any specific terms of use on the publisher's website.

**Takedown**

If you consider content in White Rose Research Online to be in breach of UK law, please notify us by emailing [eprints@whiterose.ac.uk](mailto:eprints@whiterose.ac.uk) including the URL of the record and the reason for the withdrawal request.



[eprints@whiterose.ac.uk](mailto:eprints@whiterose.ac.uk)  
<https://eprints.whiterose.ac.uk/>

DOI: 10.1002/slct.201700217

ChemistrySelect

Full Paper

Materials Science inc. Nanomaterials & Polymers

Received: 3. February.2017

Accepted: 24. February.2017

# $\pi$ -Conjugated Indole Dyads with Strong Blue Emission Made Possible by Stille Cross-Coupling and Double Fischer Indole Cyclisation

Ana M. Garrote Cañas,<sup>[a]</sup> Dr. Natalia Martsinovich,<sup>[b]</sup> and Dr. Natalia N. Sergeeva\*<sup>[a]</sup>

[a] School of Chemistry, Department of Colour Science, University of Leeds, Woodhouse Lane, Leeds, LS2 9JT, UK

[b] Department of Chemistry; University of Sheffield, Brook Hill, Sheffield, S3 7HF, UK

E-mail: [n.sergeeva@leeds.ac.uk](mailto:n.sergeeva@leeds.ac.uk)

## Abstract

Small fluorescent  $\pi$ -conjugated indolyl-based molecules **4-6**, **23** are prepared through direct Fischer synthesis or/and Stille cross-coupling method in appreciable yields. Our synthetic results have shown the benefits using Stille approach when Fischer double cyclisation method to access the bisindole dyads **4-6**, **23** is not efficient. The synthetic routes to these materials have been designed to investigate the substrate requirements for the respective cyclisation and CC-coupling reactions and to evaluate their wider synthetic applicability. Comparative analysis of the different substituents and the different  $\pi$ -bridging units e.g. pyridine, thiophene and thiazole on the electronic and photophysical properties of the final compounds **4-6**, **23** has been carried out. The structure–property relationship of the final bisindole dyads has been investigated via photophysical characterisation, and computational modelling. The obtained compounds absorb near-UV and visible (blue) light, with the spectral range dependent on the nature of the  $\pi$ -bridging units, and are of bright blue emission.

## Introduction

The role of fluorescent materials in multidisciplinary fields is recognised worldwide. This wide applicability in chemosensing<sup>[1-3]</sup>, bio-imaging<sup>[4]</sup> and devices fabrication<sup>[5]</sup> has attracted considerable scientific and industrial interest.<sup>[6,7]</sup> In particular, organic  $\pi$ -conjugated semiconductors have shown to be successful components in a range of optoelectronic devices<sup>[8-11]</sup>, including photovoltaic cells<sup>[12-15]</sup>, organic field effect transistors<sup>[16]</sup>, organic light emitting diodes (OLEDs)<sup>7,17,18]</sup> and UV detectors for scientific, commercial, civil and military<sup>[19,20]</sup> applications. Although metal free small organic molecules have rather limited  $\pi$ -conjugation, they can intrinsically display deep-blue emission as well as high fluorescence ( $\Phi$ ) yields.<sup>[18,21,22]</sup> Other advantages include precise chemical structure, high purity and high thermal stability, making them attractive targets. They can be classified based on generic scaffolds including anthracene, phenanthrene, imidazole, triphenylamine and carbazole motifs.<sup>[6,7,23]</sup> While a large number of such molecules has been developed, the increased demand in cost-effective blue-emitting materials for OLEDs commercialisation<sup>[7]</sup> highlighted a necessity of rational design and sustainable synthetic strategies to achieve the full potential of these technological applications.<sup>[24-26]</sup> Indoles are electron-rich small aromatic heterocycles widely occurring in nature. Importance of indole and its derivatives cannot be underestimated, as they often play an important role of bioactive scaffolds in biologically significant compounds.<sup>[27-33]</sup> However, their potential as fluorescence emitting materials has not been significantly explored in comparison to other popular organic chromophores.

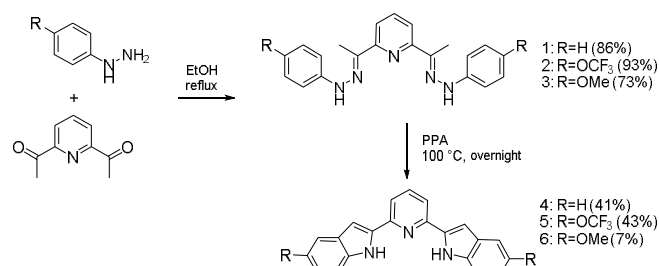
Our main objectives for this study are to explore the structure-property relationship that governs chemistry and photophysics of the indole-based blue-emitting materials. Design of  $\pi$ -conjugated materials often involves a bridging unit, which extends the conjugation, enables efficient spatial charge separation between donor and acceptor units and controls overall rigidity of the molecular framework. In this study, we have focused on pyridine, thiophene and thiazole units linked with an indole moiety bearing a donor or an acceptor group. To access

these materials, we have considered two synthetic strategies: (i) Stille coupling utilising organostannes, which are relatively stable to moisture and oxygen and can be synthesised from commercially available and cheap precursors<sup>[34,35]</sup>, and (ii) a concurrent double Fischer indole synthesis using bishydrazones. This presents a unique opportunity to investigate CC bond formation methods to access C2-functionalised indoles and to explore how the substrate requirements for these respective cross coupling reactions can influence structure–property relationship of the final indole-based dyads. These dyads' optical absorption and emission properties are then investigated, and are found to be governed by the nature of the bridging unit and the charge-transfer character of the excitations; they are also subtly influenced by the nature of the donor or acceptor substituent in the indole.

## Results and Discussion

### Fischer bis-indole synthesis

Bis(indolyl)pyridines **4** and **5** can be prepared via a two-step Fischer synthesis. The first step involves the reaction between 2,6-diacetylpyridine and two equivalents of an appropriate p-substituted phenyl hydrazine in ethanol, leading to the formation of 2,6-diacetylpyridinebis(hydrazones) **1-3** in excellent yields of 73-93%. (Scheme 1) <sup>1</sup>H NMR confirms that the compounds **1-3** exist in a sole hydrazone form in the solution. In the second step, the compounds **1-3** are cyclised in the presence of polyphosphoric acid (PPA) at 100°C into the corresponding bisindoles **4** and **5**. In the case of bishydrazone **3**, the methoxy group at the phenyl ring has a dramatic effect on the outcome of the cyclisation step. Under these established conditions, no product is formed. Alternatively, we have attempted direct hydrazone cyclisation methods either using NaOAc in HOAc or Eaton's reagent (MeSO<sub>3</sub>H/P<sub>2</sub>O<sub>5</sub>) and cyclisation strategy of in situ generated hydrazone using low melting L(+)-tartaric acid:DMU or pTSA reagents under microwave irradiation (MW295, 20 bar, 2.5 h, 120°C). However, none of the aforementioned conditions can overcome the energy barrier for bisindole **6** formation. The reaction progresses very slowly giving a rise to a semi-cyclised intermediate in the range of 10-19%, target compound **6** in the poor yield of 7% and the starting bishydrazone **3**.

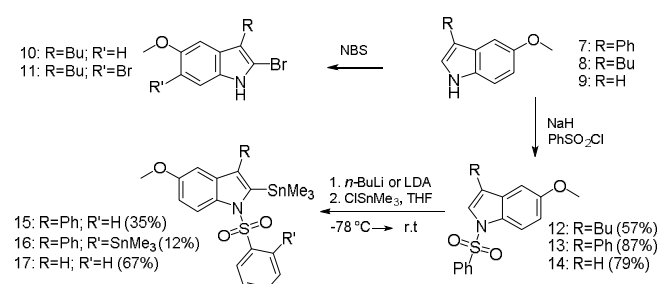


Scheme 1. Synthesis of bishydrazones **1-3** and bisindoles **4-6** via Fischer

Although this strategy yields in bisindoles **4** and **5**, it is rather limited by availability of the biscarbonyl compounds and the reaction's outcome is strongly driven by the electronic nature of substituents of the hydrazine reagents.<sup>[36,37]</sup> Thus, we have explored an alternative approach that can be used to access the target compounds.

### Functionalisation of the indole's C2 position

There is a strong preference for electrophilic substitution at the five-membered ring of the indole. We decided to exploit two alternative strategies to functionalise the C2-position: (i) via halogenation and (ii) via metalation. To investigate the full potential of both approaches, we have prepared 3-substituted indoles bearing aryl and alkyl substituents. Compounds **7** and **8** are produced via one-pot Fischer indole synthesis by simply heating the commercially available 4-methoxyphenylhydrazine and an appropriate aldehyde under acidic conditions. The choice of the acid is crucial as it determines the cyclisation rate.<sup>[38]</sup> Acids such as AcOH and H<sub>2</sub>SO<sub>4</sub> do not lead to the product formation. However, a mixture of acetic acid with NaOAc or NH<sub>4</sub>OAc, which can act as a buffer keeping the pH level relatively constant during the reaction, facilitates the cyclisation to give the 3-phenyl-1H-indole **7** and 3-butyl-1H-indole **8** in the yields of 65% and 69%, respectively. Halogenation proceeds generally at the C3-position, but if blocked, the reaction can occur at the C2-position. However, the presence of substituents in the indole may influence the course of the substitution. Halogenation of the 3-phenyl-1H-indole **7** leads to a complex mixture of dihalogenated products. 3-Butyl-1H-indole **8** results in the formation of mono- and dibrominated species **10** and **11**, respectively. Moreover, these halogenated indoles show to be very unstable, limiting their use as versatile precursors. (Scheme 2)

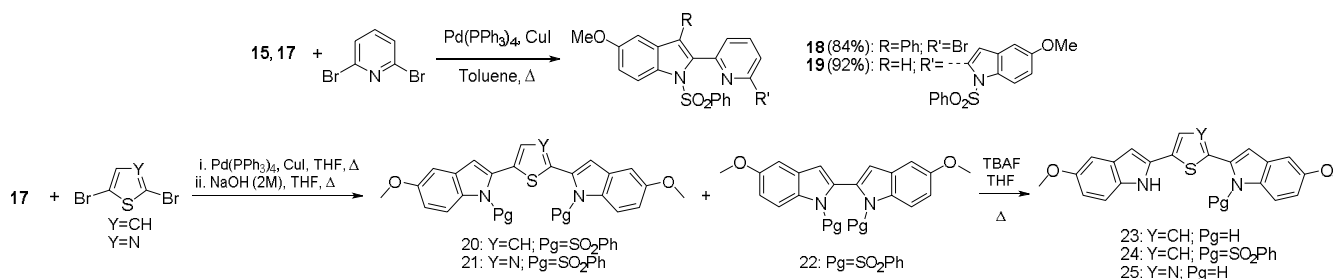


Scheme 2. Alternative synthetic routes: halogenation of the 3-substituted indoles and synthesis of 2-stanniindoles **15-17**

Consequently, we have investigated an alternative metalation route. 1,2-Bismetallated indoles cannot be directly generated due to a low reactivity of the 1-indolyl anion<sup>[39,40]</sup>, thus N-protection<sup>[41]</sup> should be carried out first. We have used PhSO<sub>2</sub>-protecting group, as its electron-withdrawing nature favours C2-regioselectivity for the generation of lithioindole derivatives. Electron rich 3-butyl-1H-indole **8** gives the N-protected indole **12** in the moderate yield of 57%. In contrast, the 3-phenyl-1H-indole **7** and 5-methoxy-1H-indole **9** can be deprotonated easily with NaH at 0°C followed by an electrophilic attack of PhSO<sub>2</sub>Cl, yielding the target indoles **13** (87%) and **14** (79%), respectively. To functionalise the C2-position, lithiation of N-protected indoles **13** and **14** with nBuLi or LDA is carried out. Subsequently, the lithiated species generated are quenched with an electrophile, such as Me<sub>3</sub>SnCl, forming the stannyl derivatives **15** and **17** in the yield of 35% and 67%, respectively. Peculiarly, an attempt to improve the yield of **15** by increasing the amount of nBuLi (over 1.4 eq) leads to the formation of compound **16**. (Scheme 2)

### Stille CC cross-coupling

To understand how structural features of the substrate can influence the outcome of the reaction and to evaluate synthetic applicability of the concurrent double Stille CC coupling, we have studied the reactivity of the 2-stannyl derivatives **15** and **17**. An attempt to perform a one-pot double Stille CC coupling between the sterically demanding 3-phenyl-2-trimethylstannylindole **15** and 2,6-dibromopyridine in a ratio 2:1 in the presence of Pd(PPh<sub>3</sub>)<sub>4</sub> and Cul in THF, leads to the formation of only the mono adduct **18** in the 84% yield. An attempt to carry out two sequential couplings to access the bisindole, reacting starting stannyl indole **15** and dibromo compound in a ratio 1:1, leads to a dramatic reduction in the yield of the mono adduct **18** from 84% to 20%. Also, a large amount of 2-unsubstituted indole **7** is recovered. Variation of the reaction conditions does not result in any further improvement of the reaction outcome and no bisindole can be formed. (Scheme 3) In contrast, bis(indolyl)derivative **6**, which is not accessible via double Fischer synthesis, can be prepared via one-pot double Stille procedure followed by deprotection. The reaction of the stannyl indole **17** with 2,6-dibromopyridine in presence of Pd(PPh<sub>3</sub>)<sub>4</sub> (10%) and Cul (20%) is shown to be very efficient, leading to bisindole **19** almost quantitatively (92%). Compound **19** can be deprotected using TBAF (3 eq) in THF under reflux yielding the target bisindole **6**. Chemical conversion for this step is 86%; however due to a low solubility of the crude mixture, the analytically pure sample can be attained in the yield of 24%.



**Scheme 3.** General synthetic strategy to the indoles **18-25** via Stille CC coupling reactions

As the nature of the bridging unit impacts on the degree of conjugation, spatial separation between the units and the rigidity of the molecular framework, we have investigated synthetic applicability of this strategy to access bisindole derivatives bearing thiophene and thiazole linking groups. The CC-coupling between the stannyl indole **17** and the corresponding 2,5-dibromothiazole is carried out in the presence of Pd(PPh<sub>3</sub>)<sub>4</sub> (20%) and Cul (20%) as co-catalysts, leading to the formation of the bisindole **21**, quantitatively. However, compound **21** appears to be extremely sensitive to light and solvents; a rapid decomposition of the thiazole compound **21** makes it impossible to carry out the deprotection step. The Stille CC-coupling between the stannyl indole **17** and the corresponding 2,5-dibromothiophene is carried out in the presence of Pd(PPh<sub>3</sub>)<sub>4</sub> (15%) and Cul (20%) to yield compound **20** in the 89% yield along with the homocoupled adduct **22**. In contrast to pyridine derivative **6**, deprotection of compound **20**, using TBAF (5 eq), leads to the formation of the desired compound **23** in the yield of 40% and compound **24** in the yield of 30%.

Thermal stability (>200°C) is required from the materials to make them suitable for any practical device fabrication. We have evaluated the thermal properties of the compounds **4-6** and **23** being able to tolerate the high temperatures. Thermal properties have been assessed by Thermogravimetric Analysis (TGA) at a heating rate of 10°C per minute under nitrogen. The compounds exhibit good thermal-stabilities and their decomposition temperatures (Td) are up to 300°C.

### Computational modelling: geometry, molecular orbitals and electronic properties

Electronic and optical properties of the compounds **4-6**, **23** and **25** have been calculated using density functional theory (DFT) calculations<sup>[42-45]</sup> and compared with experimental data. The optimized Cartesian coordinates can be found in the Supporting Information. Pyridine-based bisindoles **4-6** (later on labelled as dihydrogenated bisindole pyridine H2BIP(R), where R = H (compound **4**), OCF<sub>3</sub> (compound **5**) or OCH<sub>3</sub> (compound **6**)) have almost planar geometries (close to C<sub>2v</sub> symmetry); by comparison, the thiazole-based H2BIA(OCH<sub>3</sub>) (compound **25**) and the thiophene-based H2BIA(OCH<sub>3</sub>) (compound **23**) are non-planar and display the C<sub>2</sub> symmetry. The non-planarity can be quantified by measuring the dihedral angles between the two indole groups: all the pyridiny-based molecules **4-6** have the dihedral angles of 4-7° in MeCN (7-14° in vacuum; H2BIP(OCF<sub>3</sub>) **5** is the most non-planar of the three H2BIP molecules), compared to 17° (or 34° in vacuum) for H2BIA **25** and 38° (or 49° in vacuum) for the most nonplanar H2BIT **23** molecule. The planarity of H2BIP **4-6** may be caused by hydrogen-bonding interactions between indole imine hydrogens and the pyridine nitrogen, while hydrogen bonding to the sulphur atom in thiophene and thiazole is less likely.

Figure 1 presents the two highest occupied molecular orbitals (HOMO-1 and HOMO) and the two lowest unoccupied molecular orbitals (LUMO and LUMO+1) for each molecule (see also enlarged images in the Supporting Information). The molecular orbital plots show that the HOMO and especially the HOMO-1 of the H2BIP **4-6** are mainly localised on the indole groups (with contributions from the methoxy groups in the case of H2BIP(OCH<sub>3</sub>) **6**), while the LUMO and the LUMO+1 are mainly localised on the pyridine rings. This different localisation of the orbitals is expected to lead to charge separation in the photoexcited state. Charge separation is much less pronounced in the H2BIA **25** and H2BIT **23** molecules; the LUMO+1, LUMO and HOMO are delocalised across the whole molecule; only the (isoenergetic) HOMO-1 and HOMO-2 are localised on the indole groups and have no contributions from the thiophene or thiazole groups. The energies of the three highest occupied orbitals and the two lowest unoccupied orbitals, together with the HOMO-LUMO gap energies for all five molecules in acetonitrile solvent are shown in Figure 1. The gaps are very similar (within 0.08 eV) for all three H2BIP **4-6** molecules. There is 0.7-0.8 eV overestimation of the calculated HOMO-LUMO gaps compared to experiment (Table 1), because the calculated HOMO-LUMO gaps do not include exciton binding.<sup>[46]</sup> The gaps increase in the order H2BIP(OCH<sub>3</sub>)<H2BIP(H)<H2BIP(OCF<sub>3</sub>), in excellent

agreement with experiment; the lowest gap of H2BIP(OCH3) **6** can be attributed to delocalisation of its frontier orbitals onto the methoxy groups, while the higher gap of H2BIP(OCF3) **5** can be attributed to its non-planarity, and therefore lower conjugation in this molecule, and to the electron-withdrawing nature of the trifluoromethoxy group. H2BIA **25** and H2BIT **23** have the gap 0.5-0.6 eV smaller than the H2BIP molecules, showing the large effect of the central pyridine/thiophene/thiazole moiety. This change in the gap is mainly caused by the change in the LUMO energies (Figure 1): the thiophene and thiazole-based LUMOs are lower than the pyridine-based LUMOs. The lowest bandgap for H2BIA **25** can also explain a low light/chemical stability observed.

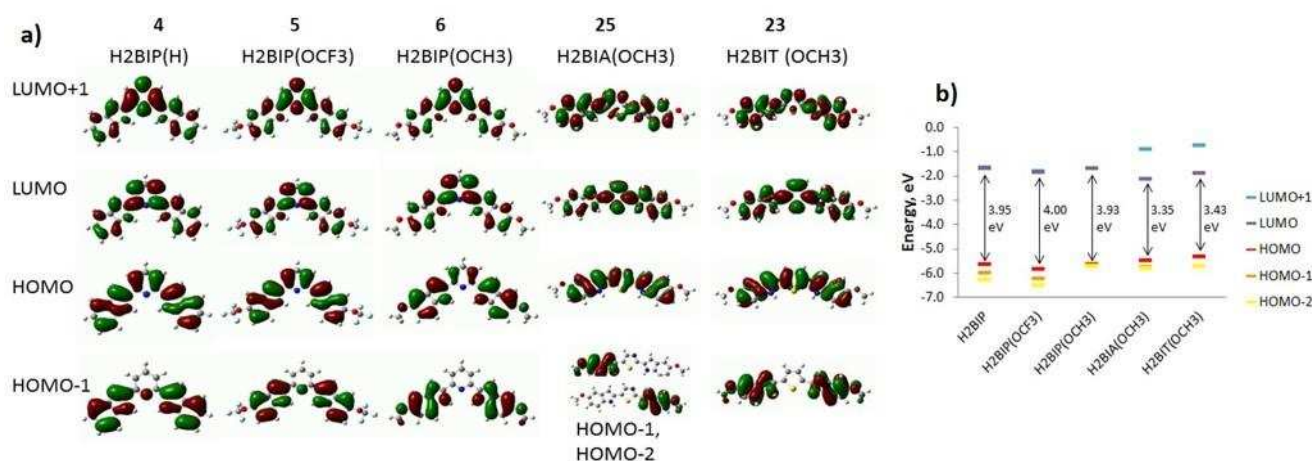


**Figure 1.** a) Molecular orbital plots for bisindoles (left to right) H2BIP(H) **4**, H2BIP(OCF3) **5**, H2BIP(OCH3) **6**, H2BIA(OCH3) **25** and H2BIT(OCH3) **23**. The LUMO+1, LUMO, HOMO and HOMO-1 are shown for the first three molecules; the HOMO-2 is additionally shown for H2BIA(OCH3) **25** (isoenergetic to the HOMO-1); the HOMO-2 of H2BIT(OCH3) **23** is also isoenergetic to its HOMO-1 and has the same shape. b) Energies of the three highest occupied orbitals and the two lowest unoccupied orbitals and the HOMO-LUMO gap energies of H2BIP **4-6**, H2BIA(OCH3) **25** and H2BIT(OCH3) **23** in acetonitrile. These orbitals are the principal contributors to the lowest-energy transitions

To investigate the competing effects of non-planarity and conjugation, an alternative structure (0.12 eV higher in energy) has been optimised for H2BIP(OCH3) **6**, with the C2 symmetry and O-C bonds of the methoxy groups not lying in the same plane as the indole rings. This structure had smaller contributions of the methoxy groups to the occupied orbitals, and consequently had lower-lying occupied orbitals; the HOMO-LUMO gap (3.96 eV) was slightly higher than for the most stable planar isomer (3.93 eV) but still below the 4.00 eV gap of H2BIP(OCF3) **5**. This shows that slight non-planarity in H2BIP(OCF3) has the effect of slightly increasing the band gap.

### Optical properties: Experimental characterisation and theoretical analysis

Absorption and emission properties of the compounds **4-6** and **23** have been studied using UV-visible (UV/vis) and fluorescence spectroscopy. The absorption spectra of the pyridine-linked series **4-6** with the electronically varied groups (H/OCH3/OCF3) display similarities in the near-blue region. (Figure 2A, Table 1) This indicates that the indole-pyridine-indole core is the dominant feature of the main absorption between 280-380 nm attributed to  $\pi$ - $\pi^*$  transitions (see the computationally predicted contributions of transitions to the overall absorption spectrum in Figure 2B). Absorption spectra for H2BIP series features a gradual enhancement of the long-wavelength band at ~345 nm (H)<(OCH3)<(OCF3). The nature of the side groups of  $\pi$ -conjugated materials can also influence the absorption efficiency, the molar absorptivity ( $\epsilon$ ) increases dramatically in the following order **4**(H)< **6**(OCH3)< **5**(OCF3). In comparison, the thiophene-linked material has an absorption onset about 80 nm lower than that of the pyridine linked material **6**. This can be largely attributed to the changes in donor-acceptor character of the thiophene bridging unit. The compounds **4-6** and **23** are capable of producing a bright blue emission upon irradiation. (Table 1, Figure 2A) The compounds of the pyridine-linked series **4-6** show similar emission profiles, with the fluorescence maxima (around 400 nm) in acetonitrile almost identical for the compounds **4**, **6** and slightly blue-shifted for the compound **5**. H2BIT **23** displays a different fluorescence spectrum and a lower onset of the emission. These changes are coherent with the theoretical calculations showing that the thiophene-linked compound undergoes larger geometric transformations upon excitation.

**Table 1.** Experimental electronic and optical properties of the bisindoles **4-6**, **23**.

	Absorbance	Emission		Bandgap eV
	$\lambda_{ab}/nm, \epsilon/M^{-1}cm^{-1}$	$\lambda_{em}, nm$	$\Phi, \%$	
<b>4</b> H2BIP(H)	320, $1.9 \times 10^4$ 347, $2.2 \times 10^4$	403	40	3.26
<b>5</b> H2BIP(OCF3)	317, $5.8 \times 10^4$ 344, $7.4 \times 10^4$	393	92	3.36
<b>6</b> H2BIP(OCH3)	352, $4.7 \times 10^4$	404	55	3.15
<b>23</b> H2BIT(OCH3)	380, $1.35 \times 10^4$	435,465	35	2.75

Efficiency of the fluorescence for the  $\pi$ -conjugated materials **4-6** and **23** is assessed through the fluorescence quantum yield ( $\Phi$ ) calculations.  $\Phi$  yield values are obtained according to the literature method<sup>[48]</sup> using anthracene and 9,10-diphenyl anthracene as cross-references; the data is summarised in Tab1. The compounds **4**, **6** and **23** give moderate  $\Phi$  yields, showing only a modest impact of the donor substituents. The best results are obtained for compound **5** bearing OCF<sub>3</sub> group; here the highest  $\Phi$  yield (0.92) of almost unity is recorded.

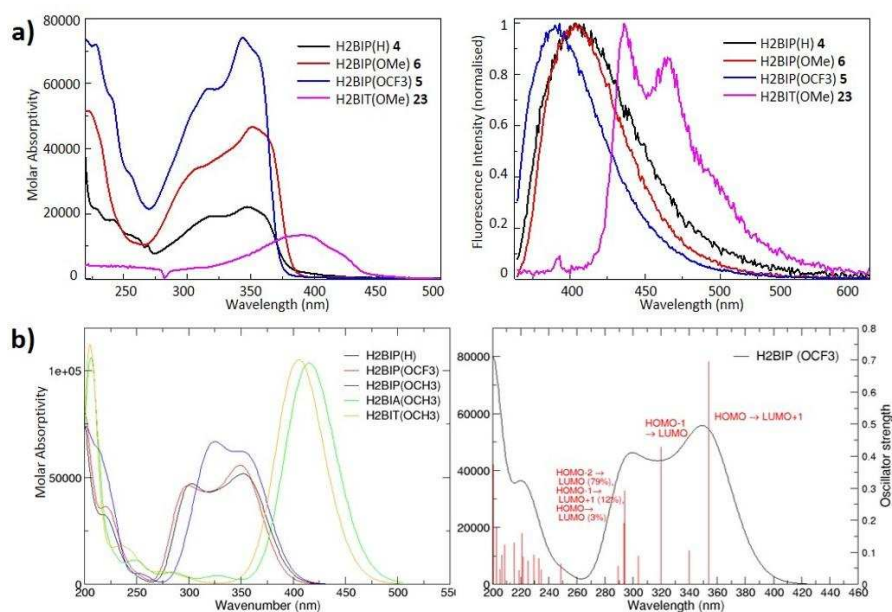


**Figure 2.** (from left to right) **a)** Experimental absorption and normalised emission spectra for **4-6** and **23** in acetonitrile. **b)** Calculated optical absorption spectra for H2BIP series **4-6**, H2BIA(OCH<sub>3</sub>) **25** and H2BIT(OCH<sub>3</sub>) **23** in acetonitrile. Principal excitations contributing to optical absorption in H2BIP(OCF<sub>3</sub>) **5**

Deviations of the fluorescence quantum yields and extinction coefficients are likely a result of subtle changes to the framework planarity, efficiency of conjugation, and donor-acceptor character of the respective peripheral units. Overall, the difference in the photophysical behaviour of these materials demonstrates the capability of the peripheral groups to fine-tune the optical properties. To help interpret the experimental results, optical absorption spectra were calculated and contributions of various excitations to the absorption spectra analysed. (Figure 2B) The spectra for all five studied molecules show two absorption bands, similar to the experiment: below 240 nm and at 280-400 nm for all H2BIP molecules **4-6**, below 220 nm and at 380-460 nm for the H2BIT **23** and H2BIA **25** molecules. From the onset of absorption in the calculated spectra, the optical gaps can be estimated as 3.11 eV, 3.15 eV, 3.10 eV, 2.70 eV and 2.62 eV for compounds **4**, **5**, **6**, **23** and **25**, respectively, in good agreement with the experimentally measured optical gaps in Table 1. Analysis of orbitals involved in photoexcitation (Figure 2B) shows that the long-wavelength band at 380-460 nm in H2BIT **23** and H2BIA **25** originates entirely from one intense HOMO→LUMO excitation; according to the molecular orbital plots, these excitations have no charge-transfer character. The shorter-wavelength band for these two molecules is a complex mixture of transitions between several occupied and unoccupied bands. The absorption spectra of the H2BIP **4-6** are more complex: the long-wavelength band for each molecule displays a double peak shape (similar to the experimental spectra). The analysis of excitation transitions shows that this double peak comes from three principal  $\pi$ - $\pi^*$  transitions: the lowest energy HOMO→LUMO+1 transition, followed by HOMO-1→LUMO, and by the excitations dominated by HOMO-2→LUMO transition. These transitions result in intramolecular charge transfer from indoles (HOMO and especially HOMO-1 and HOMO-2) to pyridine (LUMO and LUMO+1). The position of the first absorption maximum of H2BIP (352 nm) in this double peak is slightly blue shifted (353 nm) upon addition of -OCH<sub>3</sub>, because an electron-donating group, such as methoxy, destabilises or increases the HOMO energy level. By comparison, this peak is slightly blue shifted upon addition of -OCF<sub>3</sub> (349 nm), because the electron-withdrawing trifluoromethoxy group stabilises the HOMO energy level and therefore increase the HOMO-LUMO gap.<sup>[37]</sup> These subtle band shifts follow the trend in calculated band gaps and are in agreement with the experimental spectra, showing good agreement of experiment and theory and confirming applicability of the computational modelling to this class of molecules.

## Conclusions

We have studied synthetic applicability of indole molecules as versatile building blocks in the preparation of novel small  $\pi$ -conjugated materials via double Fischer synthesis and Stille CC cross-coupling protocols. The nature of their  $\pi$ -linking group and D-A characteristics of the substituents are crucial in the design of the final blue-emitting materials. Detailed investigation of both synthetic strategies gives a better understanding of the reactivity of the indole derivatives. We found that the double Fischer synthesis can be restricted both by availability of the dicarbonyl compounds and by the reactivity of the hydrazine intermediate. Alternatively, Stille cross-coupling proves to be the more efficient method as it can be expanded for the synthesis of the bisindoles bearing thiophene and thiazole bridges, otherwise unreachable via Fischer method. The key structure-property relationship of the final chromophores is revealed through different molecular designs. Donor-acceptor character and varied  $\pi$ -bridging units show a dramatic effect on the photophysical properties of the final chromophores.

Shifts in absorption/emission are defined through the nature of linking groups and the photophysical characteristics such as the extinction coefficient and quantum yield can be controlled via the structural features of bisindoles. DFT calculations support the trends recorded in the experimental observations of these compounds highlighting the reliability of the computational protocol for comparison of the related structures. The bisindoles show good thermal stability with the Td temperatures above 200°C making them suitable for organic electronics applications.

Considering this, the focus of a further work is on utilisation of these materials in the device preparation of the solution-processable OLED devices and on understanding of how the structural differences effect the device performance.

Thus, we expect that this work will assist in the design of new materials that can be synthesised through similar protocols to access functional  $\pi$ -conjugated materials for organic electronics applications.

## Supporting Information Summary

Synthetic procedures, full characterisation, the spectral data for the compounds **1-8** and **10-24** and computational calculations are described in supporting information.

## Acknowledgements

This work was supported by the Clothworker's Scholarship and the University of Leeds. NM acknowledges the use of the Sol computing cluster at the University of Sheffield.

**Keywords:** blue-emitters • computational analysis • indoles • Fischer and Stille coupling • fluorescence

- [1] R. Tang, X. Wang, W. Zhang, X. Zhuang, S. Bi, W. Zhang, F. Zhang, J. Mater. Chem. C **2016**, 4, 7640-7648.
- [2] X. Chen, F. Wang, J. Y. Hyun, T. Wei, J. Qiang, X. Ren, I. Shin J. Yoon, Chem. Soc. Rev. **2016**, 45, 2976-3016.
- [3] Y.-Z. Chen, H.-L. Jiang, Chem. Mater. **2016**, 28, 6698-6704.
- [4] T. Kowada, H. Maeda, K. Kikuchi, Chem. Soc. Rev. **2015**, 44, 4953-4972.
- [5] X. Yang, X. Xu, G. Zhou, J. Mater. Chem. C **2015**, 3, 913-944.
- [6] G. M. Farinola, R. Ragni, Chem. Soc. Rev. **2011**, 40, 3467-3482.
- [7] M. Zhu, C. Yang, Chem. Soc. Rev. **2013**, 42, 4963-4976.
- [8] A. Facchetti, Nat. Mater. **2013**, 12, 598-600.
- [9] J. E. Anthony, Nat. Mater. **2014**, 13, 773-775.
- [10] H. Sirringhaus, Nat. Mater. **2003**, 2, 641-642.
- [11] I. McCulloch, Adv. Mater. **2013**, 25, 1811-1812.
- [12] M. Kaltenbrunner, M. S. White, E. D. Glowacki, T. Sekitani, T. Someya, N. S. Sariciftci, S. Bauer, Nat. Commun. **2012**, 3, 770-777.
- [13] B. Kippelen, J.-L. Brédas, Energy Environ. Sci. **2009**, 2, 251-261.
- [14] Y.-W. Su, S.-C. Lan, K.-H. Wei, Mater. Today **2012**, 15, 554-562.
- [15] G. Li, R. Zhu, Y. Yang, Nat. Photonics **2012**, 6, 153-161.
- [16] H. Klauk, Chem. Soc. Rev. **2010**, 39, 2643-2666.
- [17] C. Groves, Nat. Mater. **2013**, 12, 597-598.
- [18] X.-H. Zhu, J. Peng, Y. Cao, J. Roncali, Chem. Soc. Rev. **2011**, 40, 3509-3524.
- [19] X. Sun, Y. Wang, Y. Lei, Chem. Soc. Rev. **2015**, 44, 8019-8061.
- [20] L. Zhang, Z. Kang, X. Xin, D. Sun, Cryst. Eng. Comm. **2016**, 18, 193-206.
- [21] L. A. Duan, L. D. Hou, T. W. Lee, J. A. Qiao, D. Q. Zhang, G. F. Dong, L. D. Wang, Y. Qiu, J. Mater. Chem. **2010**, 20, 6392-6407.
- [22] L. A. Duan, J. A. Qiao, Y. D. Sun, Y. Qiu, Adv. Mater. **2011**, 23, 1137-1144.
- [23] K.-J. Baeg, M. Binda, D. Natali, M. Caironi, Y.-Y. Noh, Adv. Mater. **2013**, 25, 4267-4295.
- [24] M. Irimia-Vladu, Chem. Soc. Rev. **2014**, 43, 588-610.
- [25] A. Marrocchi, A. Facchetti, D. Lanari, C. Petrucci, L. Vaccaro, Energy Environ. Sci. **2016**, 9, 763-786.
- [26] Z. Gao, Z. Wang, T. Shan, Y. Liu, F. Shen, Y. Pan, H. Zhang, X. He, P. Lu, B. Yang, Y. Ma, Org. Electronics **2014**, 15, 2667-2684.
- [27] T. V. Sravanthi, S. L. Manju, Eur. J. Pharm. Sci. **2016**, 91, 1-10.
- [28] C. Sherer, T. J. Snape, Eur. J. Med. Chem. **2015**, 97, 552-560.
- [29] M. Inman, C. J. Moody, Chem. Sci., **2013**, 4, 29-41.
- [30] D. F. Taber, P. K. Tirunahari, Tetrahedron, **2011**, 7195-7210.
- [31] T.-W. Chung, Y.-T. Hung, T. Thikekar, V. V. Paike, F. Y. Lo, P.-H. Tsai, M.-C. Liang, C.-M. Sun, ACS Comb. Sci. **2015**, 17, 442-451.
- [32] A. Coluccia, S. Passacantilli, V. Famiglini, M. Sabatino, A. Patsilinakos, R. Ragno, C. Mazzoccoli, L. Sisinni, A. Okuno, O. Takikawa, R. Silvestri, G. La Regina J. Med. Chem. **2016**, 59, 9760-9773.
- [33] V. Kumar, A. Bonifazi, M. P. Ellenberger, T. M. Keck, E. Pommier, R. Rais, B. S. Slusher, E. Gardner, Z.-B. You, Z.-X. Xi, A. Hauck Newman, J. Med. Chem. **2016**, 59, 7634-7650.
- [34] P. Espinet, A. M. Echavarren, Angew. Chem. 2004, 116, 4808-4839; Angew. Chem. Int. Ed. 2004, 43, 4704-4734;
- [35] C. Cordovilla, C. Bartolomé, J. M. Martínez-Illarduya, P. Espinet, ACS Catalysis **2015**, 5, 3040-3053.
- [36] N. Çelebi-Ölçüm, B. W. Boal, A. D. Hutters, N. K. Garg, K. N. Houk, J. Am. Chem. Soc. **2011**, 135, 5752-5755.
- [37] Q. Liu, M. S. Mudadu, H. Schmider, R. Thummel, Y. Tao, S. Wang, Organometallics, **2002**, 21, 4743-4749.
- [38] B. Robinson, Chem. Rev. **1963**, 63, 373-401.
- [39] D. A. Shirley, P. A. Roussel, J. Am. Chem. Soc. **1953**, 75, 375-378.
- [40] J. M. Herbert, M. Maggiani, Syn. Commun. **2001**, 31, 947-951.

- [41] R. J. Sundberg, H. F. Russell, *J. Org. Chem.* **1973**, 38, 3324-3330.
- [42] A.D. Becke, *J. Chem. Phys.* **1993**, 98, 5648-5652.
- [43] C. Lee, W. Yang, R.G. Parr, *Phys. Rev. B* **1988**, 37, 785-789.
- [44] B. Menucci, J. Tomasi, R. Cammi, J. R. Cheeseman, M. J. Frisch, F. J. Devlin, S. Gabriel, P. J. Stephens, *J. Phys. Chem. A* **2002**, 106, 6102-6113.
- [45] Gaussian 09, Revision E.01, M. J. Frisch, G. W. Trucks, H. B. Schlegel, G. E. Scuseria, M. A. Robb, J. R. Cheeseman, G. Scalmani, V. Barone, B. Mennucci, G. A. Petersson, H. Nakatsuji, M. Caricato, X. Li, H. P. Hratchian, A. F. Izmaylov, J. Bloino, G. Zheng, J. L. Sonnenberg, M. Hada, M. Ehara, K. Toyota, R. Fukuda, J. Hasegawa, M. Ishida, T. Nakajima, Y. Honda, O. Kitao, H. Nakai, T. Vreven, J. A. Montgomery, Jr., J. E. Peralta, F. Ogliaro, M. Bearpark, J. J. Heyd, E. Brothers, K. N. Kudin, V. N. Staroverov, R. Kobayashi, J. Normand, K. Raghavachari, A. Rendell, J. C. Burant, S. S. Iyengar, J. Tomasi, M. Cossi, N. Rega, J. M. Millam, M. Klene, J. E. Knox, J. B. Cross, V. Bakken, C. Adamo, J. Jaramillo, R. Gomperts, R. E. Stratmann, O. Yazyev, A. J. Austin, R. Cammi, C. Pomelli, J. W. Ochterski, R. L. Martin, K. Morokuma, V. G. Zakrzewski, G. A. Voth, P. Salvador, J. J. Dannenberg, S. Dapprich, A. D. Daniels, Ö. Farkas, J. B. Foresman, J. V. Ortiz, J. Cioslowski, and D. J. Fox, Gaussian, Inc., Wallingford CT, 2009.
- [46] E. J. Baerends, O. V. Gritsenko, R. van Meer, *Phys. Chem. Chem. Phys.* **2013**, 15, 16408-16425.
- [47] J.-L. Bredas, *Mater. Horiz.* **2014**, 1, 17-19.
- [48] J. R. Lakowicz, *Principles of Fluorescence Spectroscopy*, Ed. 3 Springer, 2006, Chp. 1, pp1-12.

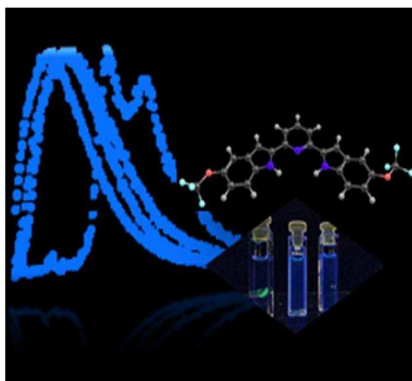
## Entry for the Table of Contents (Please choose one layout)

Layout 1:

### FULL PAPER

---

Small  $\pi$ -conjugated indole dyads are prepared via Fischer synthesis or/and Stille CC method in appreciable yields. The compounds absorb near-UV and visible light, with the spectral range dependent on the nature of the  $\pi$ -bridging units, and are capable of bright blue emission. Comparative analysis of the structure–property relationship in the bisindoles is carried out via photophysical characterisation, and via computational modelling.



Ana M. Garrote Canas, Natalia Martsinovich, and Natalia N. Sergeeva\*

**Page No. – Page No.**

**$\pi$ -Conjugated indole dyads with strong blue emission made possible by Stille cross-coupling and double Fischer indole cyclisation**

Layout 2:

### FULL PAPER

---

((Insert TOC Graphic here; max. width: 11.5 cm; max. height: 2.5 cm))

Author(s), Corresponding Author(s)\*

**Page No. – Page No.**

**Title**

Text for Table of Contents